Magnetic biosignatures of magnetosomal greigite from micromagnetic calculation

Fan Bai[1], Liao Chang[1,2], Zhaowen Pei[1], Richard J. Harrison[3], and Michael Winklhofer[4]

[1] Laboratory of Orogenic Belts and Crustal Evolution, School of Earth and Space Sciences, Peking University, 100871 Beijing, China

[2] Laboratory for Marine Geology, Qingdao National Laboratory for Marine Science and Technology, 266061 Qingdao, China

[3] Department of Earth Sciences, University of Cambridge, CB2 3EQ Cambridge, UK

[4] Institut für Biologie und Umweltwissenschaften, Carl von Ossietzky Universität Oldenburg, 26129 Oldenburg, Germany

Correspondence to: Liao Chang (liao.chang@pku.edu.cn)

Key Points:

- Micromagnetic calculations reveal robust magnetic biosignatures of biogenic greigite that have been difficult to determine experimentally
- Modelled hysteresis properties of biogenic greigite provide magnetic criteria for their identification in a wide range of environments
- Greigite-producing magnetotactic microorganisms likely have optimized their magnetic nanostructure for navigational and other purposes

This article has been accepted for publication and undergone full peer review but has not been through the copyediting, typesetting, pagination and proofreading process, which may lead to differences between this version and the Version of Record. Please cite this article as doi: 10.1029/2022GL098437.

Abstract

Greigite magnetosomes produced by magnetotactic bacteria (MTB) are widely distributed in natural environments, but large uncertainties remain regarding their magnetic biosignatures. Here, we have constructed micromagnetic models with realistic biogenic greigite particles to quantify their magnetic properties and magnetotaxis efficiency of greigite-producing MTB cells. Our calculations suggest coercivity (B_c) of ~15-21 mT for intact greigite-producing rod-shaped MTB and many-celled magnetotactic prokaryotes, with B_c decreasing to ~11 mT for greigite magnetofossils with clumped particles. These magnetic signatures make biogenic greigite distinguishable from typical biogenic magnetite and inorganic greigite, providing reliable magnetic criteria to detect biogenic greigite in a wide range of environmental and geological settings. Our numerical calculations suggest that rod-shaped greigite-producing MTB have a similar magnetotaxis efficiency to magnetite MTB, likely by biomineralizing more greigite crystals to compensate for the lower saturation magnetization of greigite and less ordered chains in greigite MTB cells, demonstrating biological-controlled optimization of their magnetic nanostructure.

Plain Language summary

Magnetic bacteria can produce greigite (Fe_3S_4) or magnetite (Fe_3O_4) nanoparticles arranged in chains and use them as nano-compass for navigating along the geomagnetic field lines. Dead magnetic bacteria can be fossilized in the geological records that retain important signals of past geomagnetic field, environmental conditions, and biochemical processes in the Earth surface. Until now magnetic biosignatures of bacterial greigite are unclear because it is difficult to obtain pure greigite MTB samples to measure their magnetic properties. Here, we constructed computer models that mimic those found in living greigite-producing magnetic bacteria. Model

calculations determined robust magnetic fingerprints of biogenic greigite that can be used to search for fossilized biogenic greigite nanoparticles in natural environments. Moreover, according to our calculations, greigite-producing magnetic bacteria have similar navigational ability to bacterial magnetite counterparts by producing more biogenic greigite crystals in the bacterial cells, suggesting that magnetic nanostructures are optimized by those magnetic microorganisms.

1. Introduction

Magnetotactic bacteria (MTB) produce intracellular ferrimagnetic crystals (magnetosomes) consisting of magnetite (Fe_3O_4) or greigite (Fe_3S_4) aligned in chains (e.g., Faivre & Schüler, 2008). These magnetosomes provide MTB a permanent magnetic dipole that orients the bacteria along geomagnetic field lines (magnetotaxis) to navigate toward optimal living conditions (Bazylinski & Frankel, 2004). Signatures from MTB can be used to trace Earth surface environmental conditions and biogeochemical cycles (e.g., Amor et al., 2020; Chen et al., 2014; Rivas-Lamelo et al., 2017). After MTB die, magnetosomes can be preserved in sediments as magnetofossils (Kopp & Kirschvink, 2008) that carry important paleomagnetic and paleoenvironmental signals (Chang et al., 2014, 2018; Roberts et al., 2011a; Vasiliev et al., 2008; Yamazaki, 2012; Yamazaki & Ikehara, 2012).

Two typical types of greigite-producing MTB have been identified over the last decades: large rod-shaped bacteria (e.g., Bazylinski et al., 1990; Heywood et al., 1990; Lefèvre et al., 2011) and many-celled magnetotactic prokaryotes (MMP; e.g., Farina et al., 1990; Mann et al., 1990; Simmons et al., 2004; Zhou et al., 2012). Previous determinations of their magnetic properties are largely based on experimental measurements (Chen et al., 2014; Kasama et al., 2006; Penninga et al., 1995; Winklhofer et al., 2007). In addition, numerical calculations were

implemented to calculate magnetic energy and magnetic moments of MMP (Acosta-Avalos et al., 2012) and critical single domain (SD) threshold sizes in greigite magnetosome chains (Muxworthy et al., 2013). Yet, the magnetic properties of greigite magnetosomes are much less known compared to the extensively investigated magnetite counterparts (e.g., Li et al., 2010; Moskowitz et al., 1989, 1993; Pan et al., 2005) and abiotic greigite crystals (e.g., Chang et al., 2007, 2008; Roberts et al., 2011b; Snowball, 1991, 1997a, 1997b; Valdez-Grijalva et al., 2018, 2020), because of the difficulties in isolating and culturing greigite MTB (Bazylinski & Frankel, 2004; Lefèvre et al., 2011) to obtain pure biogenic greigite samples. Moreover, greigite magnetosome chains often appear to be disordered and the magnetic consequences of this remain unclear. Therefore, knowledge of the magnetic biosignatures of biogenic greigite is lacking, which limits robust identifications of biogenic greigite in natural environments. As a result, the presence of greigite magnetofossils in the geological records are highly controversial (Chang et al., 2014; Reinholdsson et al., 2013; Vasiliev et al., 2008) compared to the well documented magnetite magnetofossils (e.g., Kopp & Kirschvink, 2008; Roberts et al., 2012).

Here, we construct three-dimensional micromagnetic models to calculate the magnetic properties of magnetosomal greigite. Microstructures used in our micromagnetic models are constructed directly from transmission electron microscope (TEM) observations, allowing a direct comparison with available experimental data. Effects of easy axis orientations, crystal arrangement, and collapse of greigite magnetosome chains on the magnetic properties are quantitatively investigated. Magnetotaxis efficiency for greigite MTB is quantitatively assessed.

2. Methods

2.1. Micromagnetic models

We have identified ~2000 magnetosome particles in published TEM images of greigite MTB cells (Figures 1 and S1). TEM images were processed to improve their contrast. Then the size and in-situ position of greigite magnetosomes were determined with thresholding particle-edge recognition algorithm based on the OpenCV-Python package, where we used minimum area bounding rectangle to estimate magnetosome particle size (see Text S1 in Supporting Information S1 for details). The spacing between adjacent magnetosome crystals (defined here as the distance from grain center to grain center) was calculated. Because greigite magnetosomes appear to align more randomly with respect to the chain axis (Kasama et al., 2006), we use the average nearest distance between magnetosomes as spacing (d). Morphological data of greigite magnetosomes in intact MTB cells are presented in Table S1.

Micromagnetic models were constructed based on seven TEM images (Figures 1 and S1): model rod-1 (Figures 1a and S2a), rod-2 (Figure 1b), rod-3 (Figure S1c), rod-4 (Figure S1d), rod-5 (Figure S1e), MMP-1 (Figure 1c), and MMP-2 (Figure 1d). Model rod-1-ordered was constructed with the long axis of each magnetosome aligning along the chain axis based on model rod-1 (Figures S2c and S2d). All the above models were simulated with random orientations of magnetocrystalline easy axes. Models rod-1 and rod-1-ordered were also simulated with the magnetocrystalline easy axis parallel to the elongation direction of each magnetosome in chains (Figures S2b and S2d). Models rod-1 and rod-3 were disrupted to generate: (1) model rod-1-collapsed with randomly distributed magnetosomes (d = 85 nm; Figure S2e); (2) model rod-1-clumped and rod-3-clumped with randomly distributed magnetosomes close to each other (d = 65 nm and 89 nm, respectively; Figures S2f and S3a).

We attempt to model fully disrupted chain structures as an end member considering the large variable disrupted chain structures (Amor et al., 2022; Chang et al., 2019; Pei et al., 2022).

Greigite magnetosome crystals in our models were cubo-octahedra (Figure S1c) and rectangular prisms (Figures 1 and S1; Heywood et al., 1990, 1991; Kasama et al., 2006). All models were generated using Trelis (Trelis, 2021) and meshed with an element size of 7.5 nm. Finite-element micromagnetic model MERRILL (version 1.3.3; Ó Conbhuí et al., 2018) was used to perform all micromagnetic simulations. Magnetic parameters of greigite used in the simulations are: exchange stiffness constant $A = 2\times10^{-12}$ Jm^{-1}, saturation magnetization M_s = $241\times10^{3}Am^{-1}$ (Chang et al., 2008), and magnetocrystalline anisotropy constant $K_1 = -1.7\times10^{4}$ J/m^{3} with <111> crystallographic easy axes (Winklhofer et al., 2014). ParaView (Ayachit, 2015) was used to visualize calculated domain states.

2.2. Micromagnetic calculation

We have calculated hysteresis loops, back-field isothermal remanent magnetization (IRM) curves for all models, and first-order reversal curves (FORC; Roberts et al., 2000) for model rod-2. We generated 30 (for hysteresis loops and back-field IRM curves) and 80 (for FORCs) random field directions evenly distributed over a sphere (Berndt et al., 2020) and then averaged the simulation results.

We estimated magnetotaxis efficiency using $\langle cos\,\theta \rangle$ (Frankel, 1984): $\langle cos\,\theta \rangle = coth\left(\frac{mB}{k_B T}\right) - \frac{k_B T}{mB}$, where θ is the angle between the total magnetic dipole moment $\boldsymbol{m}$ of the MTB (calculated as the vector sum of the magnetic moments of the individual magnetosomes inside the cell) and external magnetic field $\boldsymbol{B}$, k_B is Boltzmann constant, and T is temperature in Kelvin (see Text S2 in Supporting Information S1 for details).

3. Magnetic biosignatures of magnetosomal greigite: implications for their detection

All simulated curves are shown in Figures 2a, 2b, and S3-S6. Calculated back-field IRM curves for greigite magnetosomes show a gradual change (Figure 2b) compared to a sudden remanent magnetization reverse for a single chain in magnetite-producing MTB cells (Hanzlik et al., 2002; Penninga et al., 1995), but similar to those for magnetite magnetosomes in multiple strands (Hanzlik et al., 2002). This is likely because randomly aligned magnetosomes with respect to the chain axis cause incoherent magnetization rotation. In contrast, magnetosomes that are well aligned in straight single chains result in coherent magnetization rotation.

Hysteresis parameters (B_c, B_{cr}, and M_{rs}/M_s) are extracted from averaged simulated curves (Table 1). Compared to model rod-1 with random magnetocrystalline easy axis orientations, models rod-1-ordered regardless of easy axis orientations have larger variations in hysteresis parameters than those for model rod-1 with easy axis along each magnetosome elongation direction (Figure S7; Table 1). This indicates that the effect of magnetocrystalline anisotropy (K_1) on magnetic properties of greigite magnetosome chains is small (Kasama et al., 2006) compared to that of crystal arrangement. This is different to the calculated stronger K_1 effect on individual greigite particles (Winklhofer et al., 2014), which is due to magnetostatic interactions in chains (Muxworthy et al., 2013). Model rod-1-ordered with aligned easy axis has the most stable remanent state with M_{rs} mostly along the chain axis (Figures 3d and 3f) and largest B_c and B_{cr} values compared to other cases (Figures 3a-c, and 3e). Moreover, the model has the smallest value of M_{rs}/M_s (~0.5) because when shape and magnetocrystalline anisotropy are aligned, the particles behave more like randomly oriented uniaxial particles with M_{rs}/M_s of 0.5. When the two anisotropies are not aligned, it is likely increasing the availability of magnetocrystalline easy axis directions that are closer to the field, the magnetocrystalline anisotropy wins out over shape

anisotropy (Winklhofer et al., 2014). Therefore, M_{rs}/M_s values would trend larger than 0.5. When magnetosome chains are collapsed and clumped, values of B_c and B_{cr} decrease (Table 1). Hysteresis parameters for model rod-3-clumped are smaller than those for model rod-1-clumped (Table 1) because particles in model rod-3-clumped are mostly equidimensional.

A few experimental hysteresis data for greigite magnetosomes were reported. Modelled B_{cr} value (B_{cr} = 23.9 mT) in this study for the greigite MTB in Chen et al. (2014) is similar to the reported experimental coercivity data (~27.7 mT) determined from the median destructive field (MDF) of anhysteretic remanent magnetization (ARM) demagnetization curves, where their samples are dominated by greigite MTB cells. The slight difference in coercivity values is probably because ARM coercivity is generally larger than IRM coercivity (Egli, 2004). Hysteresis parameters for model rod-1-clumped and rod-3-clumped are similar to reported values for putative greigite magnetofossils within young Baltic Sea sediments (Table 1; Reinholdsson et al., 2013). For MMP models, B_{cr} values (Table 1) are similar to the experimental data on individual MMP cells (B_{cr} = 20 mT; Penninga et al., 1995) and slightly smaller than experimental data with the minimum B_{cr} = 25 mT (Winklhofer et al., 2007). Such smaller difference may be caused by: (1) The experimental B_{cr} data were measured on the in-vivo state of magnetosome chains with a straight shape in intact MMP cells (Winklhofer et al., 2007). The simulated B_{cr} values are derived from magnetosome chains in dead MMPs, where some particles deviate from the straight configuration due to cell shrinking (Shcherbakov et al., 1997). B_{cr} values for deformed chain structures are smaller than those for straight chains (Amor et al., 2022; Chang et al., 2019; Pei et al., 2022); (2) Magnetosome chain axis would have an angle with the pulsed magnetic field in situ during experiment measurements due to their particular distributions (Acosta-Avalos et al, 2012; Winkholfer et al., 2007). In contrast, modelled B_{cr} values are

averaged over randomly oriented field angles which would reduce the angle effect (Bai et al., 2021). Simulated FORC diagram for model rod-2 (Figure 2c) shows a SD peak at ~23 mT and is consistent with the experimental data in Chen et al. (2014). Moreover, the main peak is slightly offset to negative B_u axis and two low-coercivity peaks due to vortex states are asymmetric about $B_u = 0$ axis. Positive contributions below the horizontal axis are due to cubic anisotropy (Valdez-Grijalva & Muxworthy, 2019), and those above the horizontal axis are likely due to magnetostatic interactions between magnetosomes and some particles with vortex states in model rod-2 (Figure S8b).

Our simulation results provide a reasonable estimate of bulk magnetic properties of greigite-producing MTB. First, greigite magnetosomes typically have similar morphologies (i.e., cubo-octahedron and rectangular prism) in different MTB species. Second, modelled greigite magnetosomes have overall similar hysteresis parameters irrespective of their different chain structures (Figures 2d to 2f; Table 1). Moreover, most of our modelled magnetosome particles are in stable SD states (Figures S8 and S9; Muxworthy et al., 2013), indicating that thermal fluctuation, which can reduce B_c and B_{cr} values, is not expected to affect our calculated hysteresis properties. Our calculations show 'softer' biogenic greigite component (Figure 2d) compared to the magnetite 'biogenic soft' and 'biogenic hard' components identified by Egli (2004). Small dispersion parameter (DP) values are mainly due to constant length of chains and narrow grain size distribution in our models, unlike bulk natural samples containing various greigite magnetosome chains with different chain lengths and broad grain size distribution (Chen et al., 2014). Therefore, DP values for natural biogenic greigite samples are expected to be larger than our simulated DP values here and similar to that derived from ARM coercivity distribution in Chen et al. (2014) (Figure 2d).

Day plot and Néel plot (Day et al., 1977; Néel, 1955) indicate characteristic data regions for biogenic greigite. Simulated hysteresis parameters of greigite magnetosomes broadly follow the SD and MD mixing lines for inorganic magnetite (Dunlop, 2002) in the Day plot (Figure 2e). Calculated M_{rs}/M_s versus B_c data fall more to the left of the USD+SP mixing line (Tauxe et al. 2002) than those for magnetite magnetosomes in the Néel plot (Figure 2f). For intact greigite magnetosome chains, B_c values are generally in the narrow range of 15-21 mT (Figure 2f and Table 1). When chains are disrupted to form particle clumps, B_c decreases to about 11 mT. Combined with published experimental data for putative greigite magnetofossils (Chang et al., 2014; Reinholdsson, 2013; Vasiliev et al., 2008), B_c values for greigite magnetosome chains are often larger than those for synthetic ultrafine-grained superparamagnetic and coarse-grained PSD/MD greigite samples (Chang et al., 2007; Snowball, 1991), but are significantly smaller than those for typical diagenetic sedimentary SD greigite (e.g., Chang et al., 2014; Horng et al., 1992; Reinholdsson et al., 2013; Roberts et al., 2011b; Snowball, 1991, 1997a, 1997b) and biogenic magnetite (e.g., Chang et al., 2018, 2019; Kind et al., 2011; Pan et al., 2005; Roberts et al., 2011a) with the exception of bulk samples containing putative greigite magnetofossils from the Carpathian foredeep, Romania (Table 1; Vasiliev et al, 2008). Putative greigite magnetofossils were also reported with B_{cr} larger than 60 mT for sediment samples from Monte dei Corvi, northern Italy (Hüsing et al., 2009). Our modelled B_c and B_{cr} values are smaller than 21 mT and 25 mT, respectively, indicating that some reported putative greigite magnetofossils may have contributions from diagenetic greigite. Moreover, the relationship between modelled values of B_c and M_{rs}/M_s combined with data in Reinholdsson et al. (2013) can be well described by a linear function: $M_{rs}/M_s = 0.04B_c - 0.24$ (Figure 2f), which may indicate a trend of B_c and M_{rs}/M_s variation from generally intact greigite magnetosome chains to increasing degree of chain

collapse.

4. Magnetotaxis efficiency of greigite-producing MTB cells and indication on intracellular assembly of greigite magnetosomes

Our calculations show that greigite magnetosome chains of rod-shaped bacteria have a magnetotaxis efficiency with $< cos\,\theta >$ around 0.9 (Figure 4 and Table 1), similar to magnetite counterparts (Frankel & Blackmore, 1980; Klumpp et al., 2019). This indicates that despite less well-organized chains in greigite-producing MTB (Kasama et al., 2006) and the smaller M_s value of greigite (Chang et al., 2008) which reduce the cellular magnetic moment, rod-shaped greigite MTB strains biomineralize more greigite magnetosomes to form longer or multiple chains to obtain enough cellular magnetic moment for efficient magnetotaxis (Bazylinski et al, 1995; Chen et al., 2014; Kasama et al., 2006; Lefèvre et al., 2011). Rod-shaped greigite MTB species may also have optimized the maximum production of greigite magnetosome crystals, i.e., the number of magnetosomes will not increase too much once a sufficient total magnetic moment for navigation has been obtained (Figure 4), similar to magnetite MTB species (Frankel and Blackmore, 1980). This indicates that the evolution and natural selection have maximized the efficiency of magnetic orientation along the geomagnetic field in magnetic microorganisms.

Our micromagnetic simulations provide another powerful method to obtain magnetic moment of MTB in addition to experimental methods such as the u-turn method (Frankel, 1984; Kalmijn, 1981; Keim et al., 2006) and numerical calculation (Acosta-Avalos et al., 2012). Simulated total magnetic moments for MMP are about 18×10^{-15} Am^2 and 11.5×10^{-15} Am^2, respectively, which are on the same order as calculated by Winklhofer et al. (2007) and Acosta-Avalos et al. (2012). These values for MMP are one-order of magnitude larger than those for rod-shaped greigite-producing MTB (Table 1), producing $< cos\,\theta >$ close to 1 (Figure 4). This

indicates that greigite magnetosomes in MMP may serve other purposes (Kopp & Kirschvink, 2008). Moreover, MTB living in sediments require much larger magnetic moments to have efficient magnetotaxis compared to those living in water columns, which should also be taken into consideration (Mao et al., 2014).

5. Conclusions

Micromagnetic calculations indicate that greigite magnetosome chains fall within narrow hysteresis parameter regions that are distinct from their magnetite counterparts and inorganic greigite particles, making magnetic methods a useful diagnostic tool to detect magnetosomal greigite in natural environments. Our simulations indicate B_c values are in a range of 15 mT to 21 mT for chains in rod-shaped greigite-producing MTB and MMP. Values of B_c and M_{rs}/M_s would decrease to about 11 mT and 0.36 for greigite magnetofossils with clumped particles. It is found that the effect of magnetocrystalline anisotropy for greigite magnetosome chains is far less important compared to magnetosome arrangements in chains. Magnetotaxis efficiency can be assessed based on simulated magnetic moments of magnetosomes. Rod-shaped greigite MTB strains have similar magnetotaxis efficiency to magnetite MTB, indicating optimized greigite magnetosome production in MTB cells. Our study provides important magnetic criteria for biogenic greigite detection and improves understandings of the intracellular assembly of magnetosomes in greigite-producing MTB species.

Acknowledgments

This study was supported by the National Natural Science Foundation of China (NSFC grant 41974074) to L.C., and by a Royal Society-Newton Advanced Fellowship (RS-NAF) to L.C. and R.J.H. The RS-NAF grant is jointly funded by the NSFC (grant 42061130214) and the RS (grant NAF\R1\201096). We thank Nan Zhang (Peking University) for providing computing cluster for part of our micromagnetic simulations. We are grateful to Monika Korte for efficient editorial handling, Bruce Moskowitz, and an anonymous reviewer for providing constructive comments that improved this paper.

Data Availability Statement

All meshed micromagnetic models used for simulations can be downloaded from https://doi.org/10.18170/DVN/E4HQOM.

References

Acosta-Avalos, D., dos Santos Azevedo, Luciana Maria, Salama Andrade, T., & Lins de Barros, H. (2012). Magnetic configuration model for the multicellular magnetotactic prokaryote *Candidatus* Magnetoglobus Multicellularis. *European Biophysics Journal, 41*(5), 405-413. https://doi.org/10.1007/s00249-012-0789-5

Amor, M., Mathon, F. P., Monteil, C. L., Busigny, V., & Lèfevre, C. T. (2020). Iron-biomineralizing organelle in magnetotactic bacteria: Function, synthesis and preservation in ancient rock samples. *Environmental Microbiology, 22*(9), 3611-3632. https://doi.org/10.1111/1462-2920.15098

Amor, M., Wan, J., Egli, R., Carlut, J., Gatel, C., Andersen, I. M., et al. (2022). Key signatures of magnetofossils elucidated by mutant magnetotactic bacteria and micromagnetic calculations. *Journal of Geophysical Research: Solid Earth, 127*(1). https://doi.org/10.1029/2021JB023239

Ayachit, U. (2015). *The ParaView guide: A parallel visualization application*: Kitware.

Bai, F., Chang, L., Berndt, T. A., & Pei, Z. (2021). Micromagnetic calculations of the effect of magnetostatic interactions on isothermal remanent magnetization curves: implications for magnetic mineral identification. *Journal of Geophysical Research: Solid Earth, 126*(7). https://doi.org/10.1029/2021JB022335

Bazylinski, D. A., Frankel, R. B., Garratt-Reed, A. J., & Mann, S. (1991). Biomineralization of iron sulfides in magnetotactic bacteria from sulfidic environments. *Iron Biominerals* (pp. 239-255). https://doi.org/10.1007/978-1-4615-3810-3_17

Bazylinski, D. A., & Frankel, R. B. (2004). Magnetosome formation in prokaryotes. *Nature Reviews. Microbiology, 2*(3), 217-230. https://doi.org/10.1038/nrmicro842

Bazylinski, D. A., Frankel, R. B., Heywood, B. R., Mann, S., King, J. W., Donaghay, P. L., & Hanson, A. K. (1995). Controlled biomineralization of magnetite (Fe_3O_4) and greigite (Fe_3S_4) in

a magnetotactic bacterium. *Applied and Environmental Microbiology*, *61*(9), 3232-3239. https://doi.org/10.1128/aem.61.9.3232-3239.1995

Berndt, T. A., Chang, L., & Pei, Z. (2020). Mind the gap: Towards a biogenic magnetite palaeoenvironmental proxy through an extensive finite-element micromagnetic simulation. *Earth and Planetary Science Letters, 532*, 116010. http://doi.org/10.1016/j.epsl.2019.116010

Chang, L., Roberts, A. P., Muxworthy, A. R., Tang, Y., Chen, Q., Rowan, C. J., et al. (2007). Magnetic characteristics of synthetic pseudo-single-domain and multi-domain greigite (Fe_3S_4). *Geophysical Research Letters, 34*(24), L24304. https://doi.org/10.1029/2007GL032114

Chang, L., Roberts, A. P., Winklhofer, M., Heslop, D., Dekkers, M. J., Krijgsman, W., Fitz Gerald, J. D., & Smith, P. (2014). Magnetic detection and characterization of biogenic magnetic minerals: a comparison of ferromagnetic resonance and first-order reversal curve diagrams. *Journal of Geophysical Research. Solid Earth*, *119*(8), 6136-6158. https://doi.org/10.1002/2014JB011213

Chang, L., Harrison, R. J., & Berndt, T. A. (2019). Micromagnetic simulation of magnetofossils with realistic size and shape distributions: Linking magnetic proxies with nanoscale observations and implications for magnetofossil identification. *Earth and Planetary Science Letters, 527*, 115790. http://doi.org/10.1016/j.epsl.2019.115790

Chang, L., Harrison, R. J., Zeng, F., Berndt, T. A., Roberts, A. P., Heslop, D., & Zhao, X. (2018). Coupled microbial bloom and oxygenation decline recorded by magnetofossils during the Palaeocene-Eocene thermal maximum. *Nature Communications, 9*(1), 4007-9. https://doi.org/10.1038/s41467-018-06472-y

Chang, L., Vasiliev, I., van Baak, C., Krijgsman, W., Dekkers, M. J., Roberts, A. P., et al. (2014). Identification and environmental interpretation of diagenetic and biogenic greigite in sediments:

a lesson from the Messinian Black Sea. *Geochemistry, Geophysics, Geosystems, 15*(9), 3612-3627. https://doi.org/10.1002/2014GC005411

Chang, L., Winklhofer, M., Roberts, A. P., Heslop, D., Florindo, F., Dekkers, M. J., et al. (2013). Low-temperature magnetic properties of pelagic carbonates: Oxidation of biogenic magnetite and identification of magnetosome chains. *Journal of Geophysical Research: Solid Earth, 118*(12), 6049-6065. https://doi.org/10.1002/2013JB010381

Chen, A. P., Berounsky, V. M., Chan, M. K., Blackford, M. G., Cady, C., Moskowitz, B. M., et al. (2014). Magnetic properties of uncultivated magnetotactic bacteria and their contribution to a stratified estuary iron cycle. *Nature Communications, 5*(1), 4797-4797. https://doi.org/10.1038/ncomms5797

Day, R., Fuller, M., & Schmidt, V. A. (1977). Hysteresis properties of titanomagnetites: Grain-size and compositional dependence. *Physics of the Earth and Planetary Interiors, 13*(4), 260-267. http://doi.org/10.1016/0031-9201(77)90108-X

Duan, Z., Liu, Q., Gai, C., & Zhao, X. (2017). Magnetostratigraphic and environmental implications of greigite (Fe_3S_4) formation from hole U1433A of the IODP expedition 349, South China Sea. *Marine Geology, 394*, 82-97. https://doi.org/10.1016/j.margeo.2017.02.008

Dunlop, D. J. (2002). Theory and application of the day plot (M_{rs}/M_s versus H_{cr}/H_c) 1. Theoretical curves and tests using titanomagnetite data. *Journal of Geophysical Research, 107*(B3), 1-22. https://doi.org/10.1029/2001JB000486

Egli, R. (2004). Characterization of individual rock magnetic components by analysis of remanence curves, 1. unmixing natural sediments. *Studia Geophysica Et Geodaetica, 48*(2), 391-446. https://doi.org/10.1023/B:SGEG.0000020839.45304.6d

Faivre, D., & Schüler, D. (2008). Magnetotactic bacteria and magnetosomes. *Chemical Reviews, 108*(11), 4875-4898. https://doi.org/10.1021/cr078258w

Farina, M., Esquivel, D. M. S., & Lins de Barros, Henrique G. P. (1990). Magnetic iron-sulphur crystals from a magnetotactic microorganism. *Nature, 343*, 256-258. https://doi.org/10.1038/343256a0

Frankel, R. B. (1984). Magnetic guidance of organisms. *Annual Review of Biophysics and Bioengineering, 13*(1), 85-103. https://doi.org/10.1146/annurev.bb.13.060184.000505

Frankel, R. B., & Blakemore, R. P. (1980). Navigational compass in magnetic bacteria. *Journal of Magnetism and Magnetic Materials, 15-18*(3), 1562-1564. https://doi.org/10.1016/0304-8853(80)90409-6

Fu, C., Bloemendal, J., Qiang, X., Hill, M. J., & An, Z. (2015). Occurrence of greigite in the pliocene sediments of Lake Qinghai, China, and its paleoenvironmental and paleomagnetic implications. *Geochemistry, Geophysics, Geosystems, 16*(5), 1293-1306. https://doi.org/10.1002/2014GC005677

Hanzlik, M., Winklhofer, M., & Petersen, N. (2002). Pulsed-field-remanence measurements on individual magnetotactic bacteria. *Journal of Magnetism and Magnetic Materials, 248*(2), 258-267. https://doi.org/10.1016/S0304-8853(02)00353-0

Harrison, R. J., & Feinberg, J. M. (2008). FORCinel; an improved algorithm for calculating first-order reversal curve distributions using locally weighted regression smoothing. *Geochemistry, Geophysics, Geosystems, 9*(5), Q05016. https://doi.org/10.1029/2008GC001987

Heywood, B. R., Manna, S., & Frankel, R. B. (1990). Structure, morphology and growth of biogenic greigite (Fe_3S_4). *MRS Proceedings, 218*. https://doi.org/10.1557/PROC-218-93

Heywood, B. R., Bazylinski, D. A., Garratt-Reed, A., Mann, S., & Frankel, R. B. (1990). Controlled biosynthesis of greigite (Fe_3S_4) in magnetotactic bacteria. *Naturwissenschaften, 77*(11), 536-538. https://doi.org/10.1007/BF01139266

Horng, C., Chen, J., & Lee, T. (1992). Variations in magnetic minerals from two Plio-Pleistocene marine-deposited sections, southwestern Taiwan. *Journal of the Geological Society of China, 35(4), 323-335.*

Hüsing, S. K., Dekkers, M. J., Franke, C., & Krijgsman, W. (2009). The Tortonian reference section at Monte dei Corvi (Italy): evidence for early remanence acquisition in greigite-bearing sediments. *Geophysical Journal International*, *179*(1), 125-143. https://doi.org/10.1111/j.1365-246X.2009.04301.x

Jovane, L., Florindo, F., Bazylinski, D. A., & Lins, U. (2012). Prismatic magnetite magnetosomes from cultivated *Magnetovibrio blakemorei* strain MV-1: A magnetic fingerprint in marine sediments? *Environmental Microbiology Reports*, *4*(6), 664-668. https://doi.org/10.1111/1758-2229.12000

Kalmijn, A. (1981). Biophysics of geomagnetic field detection. *IEEE Transactions on Magnetics, 17*(1), 1113-1124. https://doi.org/10.1109/TMAG.1981.1061156

Kasama, T., Pósfai, M., Chong, R. K. K., Finlayson, A. P., Buseck, P. R., Frankel, R. B., & Dunin-Borkowski, R. E. (2006). Magnetic properties, microstructure, composition, and morphology of greigite nanocrystals in magnetotactic bacteria from electron holography and tomography. *The American Mineralogist, 91*(8-9), 1216-1229. https://doi.org/10.2138/am.2006.2227

Keim, C. N., Lopes Martins, J., Lins de Barros, H., Lins, U., & Farina, M. (2006). Structure, behavior, ecology and diversity of multicellular magnetotactic prokaryotes. (pp. 103-132). Springer Berlin Heidelberg. https://doi.org/10.1007/7171_040

Klumpp, S., Lefèvre, C. T., Bennet, M., & Faivre, D. (2019). Swimming with magnets: From biological organisms to synthetic devices. *Physics Reports, 789*, 1-54. https://doi.org/10.1016/j.physrep.2018.10.007

Kind, J., Gehring, A. U., Winklhofer, M., & Hirt, A. M. (2011). Combined use of magnetometry and spectroscopy for identifying magnetofossils in sediments. *Geochemistry, Geophysics, Geosystems*, 12(8). https://doi.org/10.1029/2011GC003633

Kopp, R. E., & Kirschvink, J. L. (2008). The identification and biogeochemical interpretation of fossil magnetotactic bacteria. *Earth-Science Reviews, 86*(1-4), 42-61. https://doi.org/10.1016/j.earscirev.2007.08.001

Lefèvre, C. T., Menguy, N., Abreu, F., Lins, U., Pósfai, M., Prozorov, T., et al. (2011). A cultured greigite-producing magnetotactic bacterium in a novel group of sulfate-reducing bacteria. *Science, 334*(6063), 1720-1723. https://doi.org/10.1126/science.1212596

Li, J., Pan, Y., Liu, Q., Qin, H., Deng, C., Che, R., & Yang, X. (2010). A comparative study of magnetic properties between whole cells and isolated magnetosomes of *Magnetospirillum magneticum* AMB-1. *Chinese Science Bulletin*, 55(1), 38-44. https://doi.org/10.1007/s11434-009-0333-x

Mann, S., Sparks, N. H. C., Frankel, R. B., Bazylinski, D. A., & Jannasch, H. W. (1990). Biomineralization of ferrimagnetic greigite (Fe_3S_4) and iron pyrite (FeS_2) in a magnetotactic bacterium. *Nature, 343*, 258-261. https://doi.org/10.1038/343258a0

Mao, X., Egli, R., Petersen, N., Hanzlik, M., & Zhao, X. (2014). Magnetotaxis and acquisition of detrital remanent magnetization by magnetotactic bacteria in natural sediment: first experimental results and theory. *Geochemistry, Geophysics, Geosystems, 15*(1), 255-283. https://doi.org/10.1002/2013GC005034

Monteil, C. L., & Lefèvre, C. T. (2020). Magnetoreception in microorganisms. *Trends in Microbiology, 28*(4), 266-275. https://doi.org/10.1016/j.tim.2019.10.012

Moskowitz, B. M., Frankel, R. B., Bazylinski, D. A., Jannasch, H. W., & Lovley, D. R. (1989). A comparison of magnetite particles produced anaerobically by magnetotactic and dissimilatory iron-reducing bacteria. *Geophysical Research Letters, 16*(7), 665-668. https://doi.org/10.1029/GL016i007p00665

Moskowitz, B. M., Frankel, R. B., & Bazylinski, D. A. (1993). Rock magnetic criteria for the detection of biogenic magnetite. *Earth and Planetary Science Letters, 120*(3-4), 283-300. https://doi.org/10.1016/0012-821X(93)90245-5

Muxworthy, A. R., Williams, W., Roberts, A. P., Winklhofer, M., Chang, L., & Pósfai, M. (2013). Critical single domain grain sizes in chains of interacting greigite particles; implications for magnetosome crystals. *Geochemistry, Geophysics, Geosystems, 14*(12), 5430-5441. https://doi.org/10.1002/2013GC004973

Néel, L. (1955). Some theoretical aspects of rock-magnetism. *Advances in Physics, 4*(14), 191-243. https://doi.org/10.1080/00018735500101204

Ó Conbhuí, P. O., Williams, W., Fabian, K., Ridley, P., Nagy, L., & Muxworthy, A. R. (2018). MERRILL: Micromagnetic earth related robust interpreted language laboratory. *Geochemistry, Geophysics, Geosystems, 19*(4), 1080-1106. https://doi.org/10.1002/2017GC007279

Pei, Z., Berndt, T. A., Chang, L., Bai, F., Williams, W., & Paterson, G. A. (2022). Bending and collapse: Magnetic recording fidelity of magnetofossils from micromagnetic simulation. *Journal of Geophysical Research: Solid Earth*, 127, e2021JB023447. https://doi.org/10.1029/2021JB023447

Penninga, I., de Waard, H., Moskowitz, B. M., Bazylinski, D. A., & Frankel, R. B. (1995). Remanence measurements on individual magnetotactic bacteria using a pulsed magnetic field. *Journal of Magnetism and Magnetic Materials, 149*(3), 279-286. https://doi.org/10.1016/0304-8853(95)00078-X

Pósfai, M., Buseck, P. R., Bazylinski, D. A., & Frankel, R. B. (1998). Reaction sequence of iron sulfide minerals in bacteria and their use as biomarkers. *Science, 280*(5365), 880-883. https://doi.org/10.1126/science.280.5365.880

Reinholdsson, M., Snowball, I., Zillen, L., Lenz, C., & Conley, D. J. (2013). Magnetic enhancement of Baltic Sea sapropels by greigite magnetofossils. *Earth and Planetary Science Letters, 366*, 137-150. https://doi.org/10.1016/j.epsl.2013.01.029

Rivas-Lamelo, S., Benzerara, K., Lefèvre, C. T., Monteil, C. L., Jézéquel, D., Menguy, N., Viollier, E., et al. (2017). Magnetotactic bacteria as a new model for P sequestration in the ferruginous Lake Pavin. *Geochemical Perspectives Letters, 5*, 35-41. https://doi.org/10.7185/geochemlet.1743

Roberts, A. P., Chang, L., Heslop, D., Florindo, F., & Larrasoana, J. C. (2012). Searching for single domain magnetite in the "pseudo-single-domain" sedimentary haystack: implications of biogenic magnetite preservation for sediment magnetism and relative paleointensity determinations. *Journal of Geophysical Research, 117*(B8). https://doi.org/10.1029/2012JB009412

Roberts, A. P., Chang, L., Rowan, C. J., Horng, C., & Florindo, F. (2011b). Magnetic properties of sedimentary greigite (Fe_3S_4): An update. *Reviews of Geophysics, 49*(1). https://doi.org/10.1029/2010RG000336

Roberts, A. P., Florindo, F., Villa, G., Chang, L., Jovane, L., Bohaty, S. M., Larrasoana, J. C., Heslop, D., & Fitz Gerald, J. D. (2011a). Magnetotactic bacterial abundance in pelagic marine environments is limited by organic carbon flux and availability of dissolved iron. *Earth and Planetary Science Letters, 310*(3-4), 441-452. https://doi.org/10.1016/j.epsl.2011.08.011

Roberts, A. P., Pike, C. R., & Verosub, K. L. (2000). First- order reversal curve diagrams: A new tool for characterizing the magnetic properties of natural samples. *Journal of Geophysical Research, 105*(B12), 28461-28475. http://doi.org/10.1029/2000JB900326

Shcherbakov, V. P., Winklhofer, M., Hanzlik, M., & Petersen, N. (1997). Elastic stability of chains of magnetosomes in magnetotactic bacteria. *European Biophysics Journal, 26*(4), 319-326. https://doi.org/10.1007/s002490050086

Simmons, S. L., Sievert, S. M., Frankel, R. B., Bazylinski, D. A., & Edwards, K. J. (2004). Spatiotemporal distribution of marine magnetotactic bacteria in a seasonally stratified coastal salt pond. *Applied and Environmental Microbiology, 70*(10), 6230-6239. https://doi.org/10.1128/AEM.70.10.6230-6239.2004

Snowball, I. F. (1991). Magnetic hysteresis properties of greigite (Fe_3S_4) and a new occurrence in Holocene sediments from Swedish Lappland. *Physics of the Earth and Planetary Interiors, 68*(1-2), 32-40. https://doi.org/10.1016/0031-9201(91)90004-2

Snowball, I. F. (1994). Bacterial magnetite and the magnetic properties of sediments in a Swedish lake. *Earth and Planetary Science Letters, 126*(1-3), 129-142. https://doi.org/10.1016/0012-821X(94)90246-1

Snowball, I. F. (1997a). Gyroremanent magnetization and the magnetic properties of greigite-bearing clays in southern Sweden. *Geophysical Journal International, 129*(3), 624-636. https://doi.org/10.1111/j.1365-246X.1997.tb04498.x

Snowball, I. F. (1997b). The detection of single-domain greigite (Fe_3S_4) using rotational remanent magnetization (RRM) and the effective gyro field (Bg): Mineral magnetic and palaeomagnetic applications. *Geophysical Journal International, 130*(3), 704-716. https://doi.org/10.1111/j.1365-246X.1997.tb01865.x

Tauxe, L., Bertram, H. N., & Seberino, C. (2002). Physical interpretation of hysteresis loops: micromagnetic modeling of fine particle magnetite. *Geochemistry, Geophysics, Geosystems, 3*(10), 1-22. https://doi.org/10.1029/2001GC000241

Trelis (Version 2021.3) [Computer software]. Orem, UT: Coreform LLC. Retrieved from http://coreform.com

Valdez-Grijalva, M. A., & Muxworthy, A. R. (2019). First-order reversal curve (FORC) diagrams of nanomagnets with cubic magnetocrystalline anisotropy: A numerical approach. *Journal of Magnetism and Magnetic Materials, 471*, 359-364. https://doi.org/10.1016/j.jmmm.2018.09.086

Valdez-Grijalva, M. A., Muxworthy, A. R., Williams, W., O Conbhui, P., Nagy, L., Roberts, A. P., & Heslop, D. (2018). Magnetic vortex effects on first-order reversal curve (FORC) diagrams for greigite dispersions. *Earth and Planetary Science Letters, 501*, 103-111. https://doi.org/10.1016/j.epsl.2018.08.027

Valdez-Grijalva, M. A., Nagy, L., Muxworthy, A. R., Williams, W., Roberts, A. P., & Heslop, D. (2020). Micromagnetic simulations of first-order reversal curve (FORC) diagrams of framboidal greigite. *Geophysical Journal International, 222*(2), 1126-1134. https://doi.org/10.1093/gji/ggaa241

Vasiliev, I., Franke, C., Meeldijk, J. D., Dekkers, M. J., Langereis, C. G., & Krijgsman, W. (2008). Putative greigite magnetofossils from the Pliocene epoch. *Nature Geoscience, 1*(11), 782-786. https://doi.org/10.1038/ngeo335

Winklhofer, M., Abraçado, L. G., Davila, A. F., Keim, C. N., & Lins de Barros, H. G. P. (2007). Magnetic optimization in a multicellular magnetotactic organism. *Biophysical Journal*, *92*(2), 661-670. https://doi.org/10.1529/biophysj.106.093823

Winklhofer, M., Chang, L., & Eder, S. H. K. (2014). On the magnetocrystalline anisotropy of greigite (Fe_3S_4). *Geochemistry, Geophysics, Geosystems*, *15*(4), 1558-1579. https://doi.org/10.1002/2013GC005121

Yamazaki, T. (2012). Paleoposition of the intertropical convergence zone in the eastern Pacific inferred from glacial-interglacial changes in terrigenous and biogenic magnetic mineral fractions. *Geology, 40*(2), 151-154. https://doi.org/10.1130/G32646.1

Yamazaki, T., & Ikehara, M. (2012). Origin of magnetic mineral concentration variation in the Southern Ocean. *Paleoceanography*, *27*(2). https://doi.org/10.1029/2011PA002271

Pan, Y., Petersen, N., Winklhofer, M., Davila, A. F., Liu, Q., Frederichs, T., Hanzlik, M., & Zhu, R. (2005). Rock magnetic properties of uncultured magnetotactic bacteria. *Earth and Planetary Science Letters*, *237*(3-4), 311-325. https://doi.org/10.1016/j.epsl.2005.06.029

Zhou, K., Zhang, W., Yu-Zhang, K., Pan, H., Zhang, S., Zhang, W., Yue, H., Li, Y., Xiao, T., & Wu, L. (2012). A novel genus of multicellular magnetotactic prokaryotes from the Yellow Sea. *Environmental Microbiology*, *14*(2), 405-413. https://doi.org/10.1111/j.1462-2920.2011.02590.x

Figure 1. Transmission electron microscopy (TEM) images of greigite-producing MTB (left in each subplot): (a) reprinted from Chen et al. (2014), Copyright 2014, with permission from Springer Nature, (b) reprinted from Heywood et al. (1990), Copyright 1990, with permission from Springer Nature, (c) reprinted from Monteil & Lefèvre (2020), Copyright 2020, with permission from Elsevier, and (d) reprinted from Winklhofer et al. (2007), Copyright 2007, with permission from Elsevier. The corresponding constructed micromagnetic models (right in each subplot) are rod-1, rod-2, MMP-1, and MMP-2, respectively. Scale bars for models and TEM images are the same.

Figure 2. (a, b) Averaged simulated hysteresis loops and back-field IRM curves. (c) Simulated FORC diagram processed using FORCinel (Harrison and Feinberg, 2008) for model rod-2 with a smoothing factor of 5. (d) Summary of DP against B_{cr} for our simulation results, uncultivated greigite-producing MTB in Chen et al. (2014), and biogenic magnetite components (biogenic soft, BS; biogenic hard, BH) identified by Egli (2004). Data point of Chen et al. (2014) is derived from ARM coercivity distribution. The blue arrow means DP values for bulk greigite MTB samples are likely larger than our modelled results. Gray areas are 95% confidence ellipse. (e, f) Day plot (Day et al., 1977) and Néel plot (Néel, 1955) with mixing lines for magnetite following Dunlop et al. (2002) and Tauxe et al. (2002), respectively. Data points in the plots are our modelling results and published experimental data: putative greigite magnetofossils (square, Reinholdsson et al., 2013; triangle, Chang et al., 2014; diamond, Vasiliev et al., 2008), sedimentary SD greigite (Chang et al., 2014; Duan et al., 2017; Fu et al., 2015; Horng et al., 1992; Reinholdsson et al., 2013; Snowball, 1991, 1997a, 1997b), synthetic greigite (Chang et al., 2007; Snowball, 1991), and magnetosomal magnetite (Chang et al., 2018; Jovane et al., 2012; Kind et al., 2011; Li et al., 2010; Moskowitz et al., 1989; Pan et al., 2005; Roberts et al., 2011a;

Snowball, 1994). Black solid line in (f) indicates trend defined by a linear function with 95% confidence interval (gray area) for our simulation results and experimental data in Reinholdsson et al. (2013). CSD, cubic single domain; USD, uniaxial single domain; SP, superparamagnetic.

Figure 3. Calculated remanent domain states at saturated field (a-d) and switching field B_{cr} (e-f) for model rod-1 and rod-1-ordered: (a, c, and e) models with random orientations of easy axes, (b, d, and f) models with the easy axis orientation along the particle elongation direction. Color bar illustrates angles between the remanent magnetization and the chain axis.

Figure 4. Calculated alignment $< cos\theta >$ of magnetosome chains with the geomagnetic field (30 μT) for different modelled greigite magnetosome chains at room temperature.

Table 1. Calculated hysteresis parameters and degree of magnetic alignment for different modelled greigite magnetosome chains and experimental data.

Greigite magnetosomes	B_c (mT)	B_{cr} (mT)	M_{rs}/M_s	m (10^{-15}Am^2)	$\langle \cos\theta \rangle$
Micromagnetic models					
Rod-1 (random easy axis orientations)	20.3	23.9	0.61	2.19	0.94
Rod-1 (easy axis along elongation directions of magnetosomes)	21.8	25.4	0.59	–	0.94
Rod-1-ordered (random easy axis orientations)	23.0	29.0	0.55	–	0.94
Rod-1-ordered (easy axis along elongation directions of magnetosomes)	26.6	30.7	0.51	–	0.95
Rod-1-collapsed	18.7	23.1	0.68	–	–
Rod-1-clumped	15.6	21.4	0.45	–	–
Rod-2	18.8	23.2	0.51	1.42	0.91
Rod-3	18.0	21.9	0.51	1.58	0.91
Rod-3-clumped	11.2	15.4	0.36	–	–
Rod-4	17.1	19.8	0.51	2.26	0.94
Rod-5	18.1	20.7	0.52	3.22	0.96
MMP-1	15.1	18.1	0.57	~18.0 (~0.044 per crystal)	~0.99
MMP-2	17.3	20.7	0.53	~11.5 (~0.034 per crystal)	~0.99
Experimental data					
Putative greigite magnetofossils (Reinholdsson et al., 2013)	13 ± 2	25 ± 2	0.3 ± 0.1	–	–
Putative greigite magnetofossils (Vasiliev et al., 2008)	28.8	62.4	0.3	–	–
Putative greigite magnetofossils (Hüsing et al., 2009)	–	>60	–	–	–

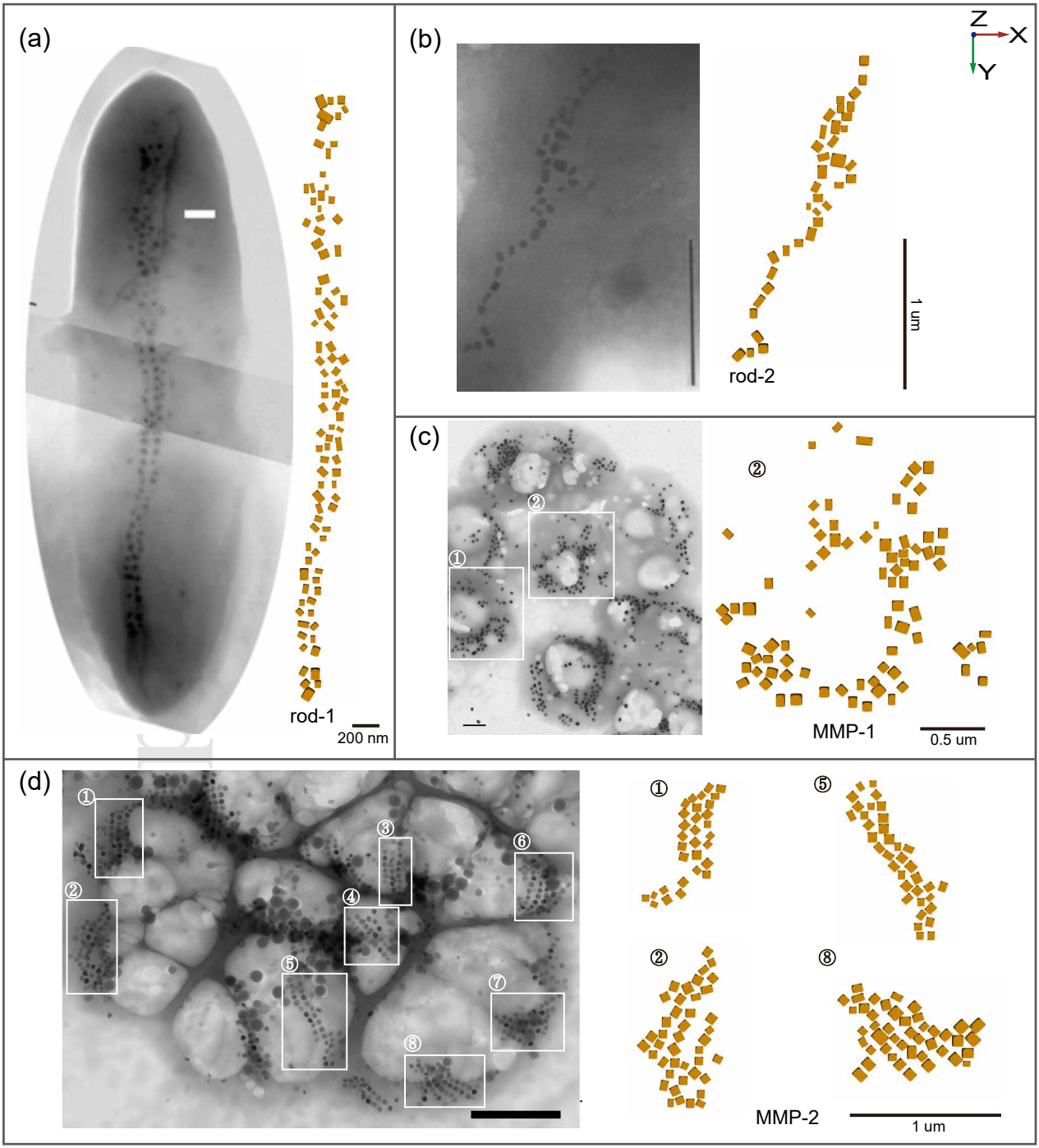
(a)
rod-1
200 nm
(b)
Z
X
Y
rod-2
1 um
(c)
①
②
②
MMP-1
0.5 um
(d)
①
②
③
④
⑤
⑥
⑦
⑧
①
②
⑤
⑧
MMP-2
1 um

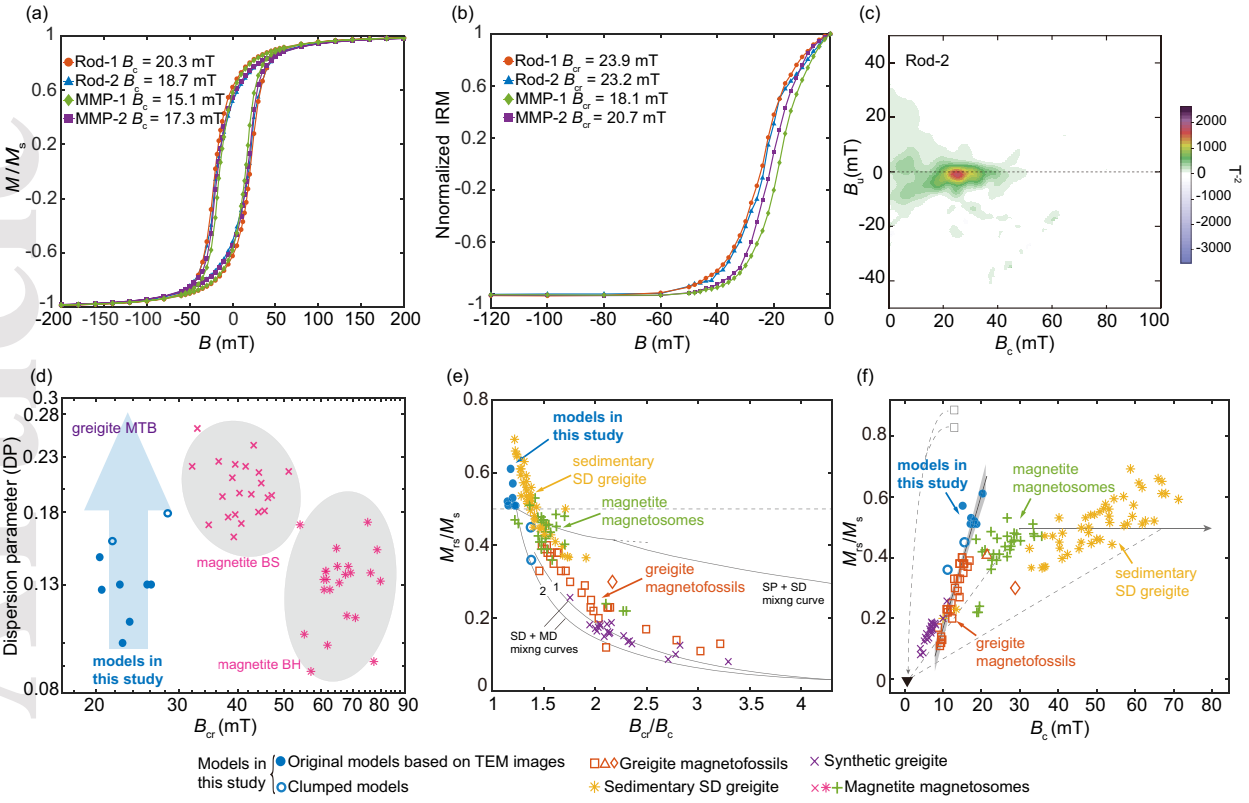

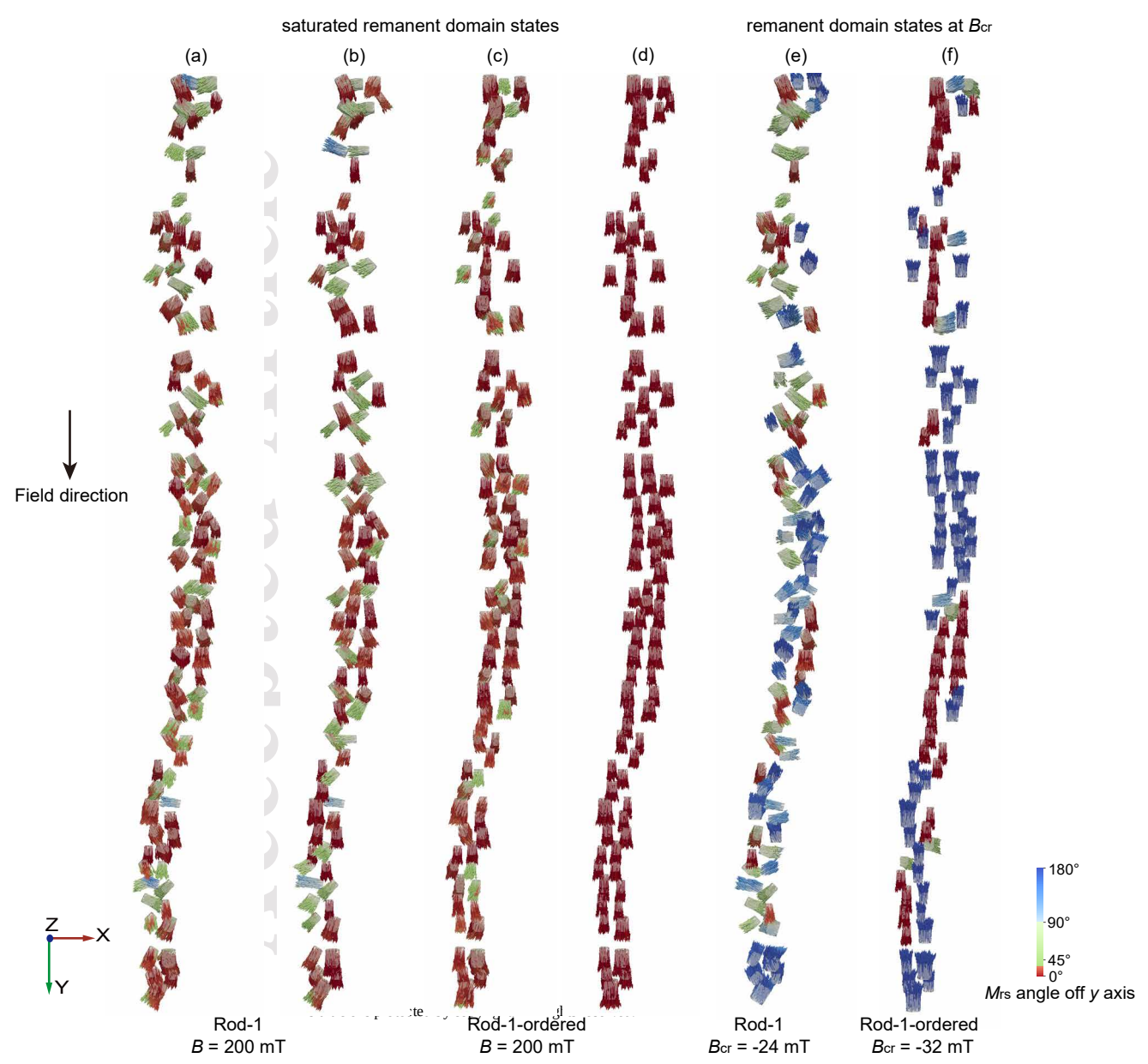
saturated remanent domain states
remanent domain states at B_{cr}
(a)
(b)
(c)
(d)
(e)
(f)
Field direction
Z
X
Y
180°
90°
45°
0°
M_{rs} angle off y axis
Rod-1
B = 200 mT
Rod-1-ordered
B = 200 mT
Rod-1
B_{cr} = -24 mT
Rod-1-ordered
B_{cr} = -32 mT